Subdiffusive spreading of a Bose-Einstein condensate in random potentials

Bin Min* and Tiejun Li†
Beijing International Center for Mathematical Research (BICMR), and LMAM and School of Mathematical Sciences, Peking University, Beijing 100871, People's Republic of China

Matthias Rosenkranz and Weizhu Bao‡
Department of Mathematics, National University of Singapore, 119076, Singapore

(Received 12 January 2012; revised manuscript received 17 August 2012; published 14 November 2012)

We study numerically the long-time dynamics of a one-dimensional Bose-Einstein condensate expanding in a speckle or impurity disorder potential. Using the mean-field Gross-Pitaevskii equation, we demonstrate subdiffusive spreading of the condensate for long times. We find that interaction-assisted hopping between normal modes leads to this subdiffusion. A possible (partial) reason why the root-mean-square (rms) width saturates in the experiment [Nature (London) **453**, 891 (2008)] is provided. We suggest that observing both the participation length and the rms width of a condensate, rather than only the rms width, could provide a more complete description of the long-time behavior of ultracold atoms in disorder potentials. Our study confirms subdiffusive spreading in spatially continuous disordered interacting models and highlights new features which spatially discrete models do not possess.

DOI: 10.1103/PhysRevA.86.053612 PACS number(s): 03.75.Kk, 05.60.−k, 03.75.Lm, 03.75.Nt

I. INTRODUCTION

One-particle wave functions in disordered media undergo Anderson localization (AL) if the disorder potential is sufficiently strong [1]. However, it is a long-standing puzzle how interactions affect AL in disordered media [2–4]. This issue arises in various physical systems, including metals and superconductors [5,6], lights in disordered media [7,8], and disordered quantum gases [4,9,10]. In the last 20 years, it has been hotly debated whether localization survives in interacting quantum systems on long time scales [11–19]. Modelling a random disorder potential with spatially discrete models such as the discrete nonlinear Schrödinger equation (DNLSE), it was found that eventually interactions lead to subdiffusion of the whole or parts of the wave packet [11–17]. In contrast, spatially continuous models still lack numerical long-time studies [20,21].

Bose-Einstein condensates (BECs) with tunable interactions are very promising systems to address the AL problem in experiments [9,10,22–26]. For instance, groups in Orsay and Florence observed AL of a BEC in a speckle potential [22] and a quasiperiodic lattice [23], respectively. More recently, the Florence group observed subdiffusion in a BEC of interacting ^{39}K atoms trapped in a quasiperiodic potential [26]. However, the subdiffusion phenomenon has not been observed in any experiment described by spatially continuous models.

In this article, we address the long-time dynamics of a (continuous) one-dimensional (1D) mean-field BEC expanding in a speckle potential. Whereas the BEC appears to localize at short times, an open problem posed in Ref. [20] is this: How do residual interactions affect the localized state at long times? Our numerical data support the solution that residual interactions destroy the localized state, eventually. Moreover, the transport is subdiffusive for long times. We also confirm subdiffusion in a correlated impurity disorder potential and with generalized short-range interactions. We explain the origin of this subdiffusive spreading as interaction-assisted hopping between normal modes (NMs). A possible reason why root-mean-square (rms) width saturates in the experiment [22] is provided. We argue that it would be advantageous to measure the participation length in addition to the rms width for studying subdiffusion in ultracold atom experiments. In sharp contrast to spatially continuous models, we find that AL is destroyed in the tails for generic coupling constants in our model indicating a possible breakdown for existing subdiffusion theories [14,26]. Our study complements previous works on spatially discrete models and highlights new features which these models do not possess.

The paper is organized as follows. In Sec. II we will give a detailed description of the model we investigated and the numerical method we used. The subdiffusion phenomenon observed in the speckle potential will be presented in Sec. III. In Sec. IV we will develop a heuristic model to explain the subdiffusion phenomenon. A discussion about the experiment [22] will be presented in Sec. V. In Sec. VI, the generalized interactions and an impurity model of disorder are considered. We then conclude the paper with a summary in Sec. VII.

II. THE MODEL AND NUMERICAL METHOD

We consider a trapped, 1D BEC with weak short-range interactions characterized by the coupling constant $g = 2\hbar\omega_\perp a_s$, where $\omega_\perp$ is the radial trapping frequency and a_s is the (three-dimensional) s-wave scattering length. We assume a harmonic trapping potential $m\omega^2 z^2/2$ plus a disorder potential $V(z)$, where m is the atom mass and ω is the trapping frequency. We consider a speckle potential $V(z) = V_R v(z/\sigma_R)$ (see an impurity model of disorder in Sec. VI) [20,22,27,28]. Here, v has a single point density function

$$\mathcal{P}(v) = \begin{cases} \exp(-v-1) & \text{if } v \geqslant -1, \\ 0 & \text{otherwise,} \end{cases}$$

*minbmath@gmail.com
†tieli@pku.edu.cn
‡bao@math.nus.edu.sg

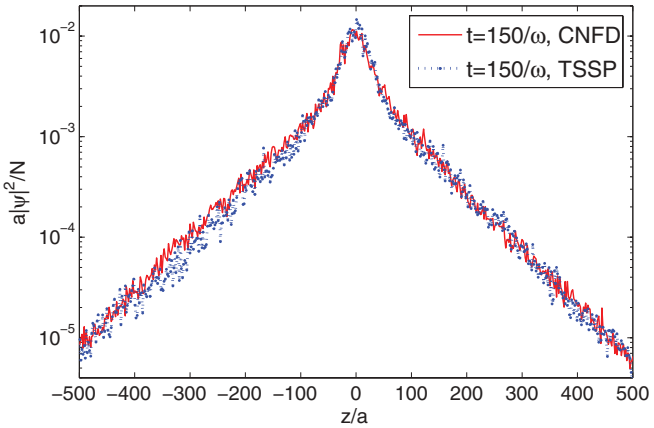

FIG. 1. (Color online) Averaged BEC density profiles after $t = 150/\omega$ in a speckle potential. The densities are averages of $|\psi|^2$ over 10 realizations in the interval with width $0.2a$, where $a = (\hbar/m\omega)^{1/2}$. The curves for $t = 150/\omega$ were computed with the CNFD (red solid) and TSSP algorithms (blue dot), respectively. The parameters are $V_R = 0.12\mu, \hbar\omega = 0.024\mu, \sigma_R = 0.65\xi_{\rm in}$. The space grid is $\Delta z = 1.2\sigma_R$ and time grids are $\Delta t = 0.00005/\omega$ (CNFD algorithm) and $\Delta t = 0.002/\omega$ (TSSP).

and correlation function $C_v(z) = \sin^2(z)/z^2$. At zero temperature, the BEC wave function $\psi = \psi(z,t)$ is governed by the Gross-Pitaevskii equation (GPE)

$$i\hbar\partial_t\psi = \left[-\frac{\hbar^2}{2m}\partial_z^2 + \frac{m\omega^2 z^2}{2} + V(z) + g|\psi|^2\right]\psi, \quad (1)$$

where $\int |\psi|^2 dz = N$ with N the total number of atoms [29]. In our simulations, initially the BEC is prepared in the ground state of Eq. (1). At $t = 0$, the harmonic potential is switched off (ω is set to 0) so the BEC evolves in the disorder potential. Here, we only focus on the regime $\sigma_R < \xi_{\rm in}$ where $\xi_{\rm in} = \hbar/\sqrt{4m\mu}$ is the healing length and μ is the chemical potential.

We use the time splitting spectral (TSSP) method for computing this evolution. The TSSP algorithm is highly efficient for solving the GPE with weak to moderate repulsive interaction [30,31]. We have compared intensively the TSSP algorithm with the Crank-Nicolson finite difference (CNFD) algorithm commonly used in the disordered quantum gas community [20,27,28]. The matching BEC density profiles for both TSSP and CNFD in Fig. 1 show that a space grid size $\Delta z/\sigma_R \sim 1$ is sufficient for the computation. However, the smaller time step Δt required for the CNFD algorithm severely limits the total simulation time. For example, for $\Delta z/\sigma_R \sim 1$ and total time $t = 150/\omega$ we require a time step $\Delta t = 0.00005/\omega$ for CNFD but only $\Delta t = 0.002/\omega$ for TSSP (see Fig. 1). It takes about two months with the TSSP method on one CPU core at 2.26 GHz to calculate up to $t = 10^5/\omega$ in the parameter regime of Ref. [22]. However, it is a formidable task to calculate up to this time scale with the CNFD method. On a technical note, TSSP is symplectic and time reversible, which is more efficient and robust than CNFD for handling long-time simulations [30,32].

III. SUBDIFFUSION EXPANSION IN A SPECKLE POTENTIAL

In previous works, the BEC expansion above was explained by a toy model with two stages [20,22]. In the first, interaction-dominated stage, the BEC evolves into the final stationary momentum distribution

$$\mathcal{D}(k) \triangleq |\hat{\psi}(k)|^2 = \frac{3N\xi_{\rm in}}{4}[1-(k\xi_{\rm in})^2]\Theta[1-(k\xi_{\rm in})^2], \quad (2)$$

where Θ is the Heaviside step function. In the second stage, the interaction is assumed to vanish and the BEC is treated as the superposition of noninteracting NMs with population $\mathcal{D}(k)$. We investigated numerically the assumption of the second stage up to long time scales ($10^5/\omega$). We set the contact interaction g to zero after a short time and let the BEC evolve to a long final time. The magenta line in the top panel of Fig. 2 shows that the resulting density profile differs significantly from the profile when g is not set to zero (red line). Therefore, this heuristic two-stage model significantly underestimates the spreading caused by the residual interactions at long times [33].

We have observed two new features in the density profiles at long time scales (see the top panel of Fig. 2). First, the slope of the exponential tails decreases in time, in contrast to constant slope in the cubic DNLSE [12,13]. The decreasing

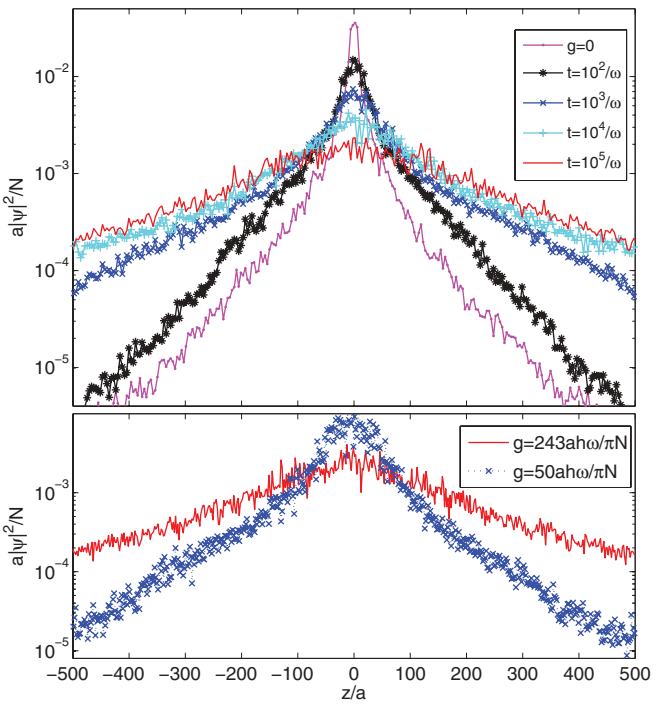

FIG. 2. (Color online) Averaged BEC density profiles after various expansion times in a speckle potential. The densities are averages of $|\psi|^2$ over 7 realizations in the interval with width $0.4a$, where $a = (\hbar/m\omega)^{1/2}$. Top panel: Density profiles at $t = 10^2/\omega, 10^3/\omega, 10^4/\omega, 10^5/\omega$ (from bottom to top at $z/a = 500$). The magenta line (bottom line at $z/a = 250$): The contact interaction was set to 0 after $t_0 = 10/\omega$ for total evolution time $t = 10^5/\omega$. The parameters are $V_R = 0.12\mu, \hbar\omega = 0.024\mu$ (i.e., $g = 243a\hbar\omega/\pi N$), $\sigma_R = 0.65\xi_{\rm in}$. Bottom panel: Development of a central plateau in the density profiles at $t = 3\times 10^4/\omega$ with small coupling constant. Other parameters are $V_R = 4.85\hbar\omega, \sigma_R = 0.051a$.

slope indicates that in our model AL is destroyed in the tails for long times. We explain this destruction as follows. The localization length of NMs within the Born approximation is

$$\xi(\epsilon) = \frac{4\hbar^2}{\pi m}\frac{\epsilon}{V_R^2\sigma_R}\frac{1}{(1-k\sigma_R)}\frac{1}{\Theta[1-(k\sigma_R)^2]}, \qquad (3)$$

where $k = \sqrt{2m\epsilon}/\hbar$ [10,34]. According to Eq. (2), there are a considerable number of NMs with large localization length in the tails when the coupling constant g is large enough. Therefore, the destruction of AL in the tails is most likely a consequence of strong interaction of NMs with large localization length in the tails. Another notable feature of the profiles is that there is no chapeau in the center of the wave packet, in contrast to its existence in the cubic DNLSE [12,13]. This difference is also related to the strong interaction between NMs with large localization length in the tails in our model. A way to test this claim is to decrease the coupling constant g because smaller g would excite NMs with smaller localization length. Indeed, the bottom panel of Fig. 2 shows that a prominent chapeau develops for smaller g. This also indicates that the tail is driven by NMs from the chapeau when NMs with large localization length in the tails are suppressed, which validates the heuristic model we will develop in Sec. IV when g is small. We note that these two features were also observed and explained in Klein-Gordon chains when the nonlinearity exponent is very small [35].

We use the rms width $L(t) = \sqrt{\langle z^2\rangle - \langle z\rangle^2}$ and participation length $P(t) = 1/\int |\psi(z,t)|^4 dz$ to characterize the spreading of the BEC. The participation length measures the typical width of a wave packet [8,13,36]. We present the evolution of L and P in the top panel of Fig. 3. L and P clearly show a power-law behavior

$$L(t) \sim t^{\alpha_1}, \quad P(t) \sim t^{\alpha_2}, \quad \alpha_1,\alpha_2 < 1/2 \qquad (4)$$

up to $t = 10^5/\omega$. We find that the subdiffusion exponents α_1 and α_2 are about $0.2 \sim 0.3$ by fitting the numerical data in the time interval $[10^2, 10^5]$ over 7 realizations [37]. Because $\alpha_{1,2} < 1/2$, we conclude that the BEC spreads subdiffusively. The difference between α_1 and α_2 indicates inhomogeneous spreading of the wave packet also observed in the DNLSE model [38]. We note that subdiffusive spreading is preserved for long times in our simulations when the external parameters, such as the coupling constant g, the speckle amplitude V_R, and the correlation length σ_R, are varied in a relatively large regime.

Now we investigate the effect of the sign of the nonlinearity on the spreading of the BEC. In discrete models, two opposing regimes exist irrespective of the sign of the nonlinearity: the self-trapping and subdiffusive regimes [13–15]. Self-trapping can be identified by the saturation of P [13–15]. In our continuous model we only find self-trapping for attractive interactions as illustrated in the bottom panel of Fig. 3. To explain this behavior we consider the total energy $E_{\rm tot}(t) = \langle\psi,\mathcal{L}\psi\rangle + g\int|\psi|^4 dz$. The spectrum of the operator $\mathcal{L}$ is bounded from below by $-V_R$. Therefore, $\langle\psi,\mathcal{L}\psi\rangle > (-V_R)\int|\psi|^2 dz = -NV_R$. Assume that

$$\sup_z |\psi(z,t)|^2 \to 0 \quad \text{for} \quad t\to\infty. \qquad (5)$$

Then $\int|\psi|^4 dz \leqslant \sup_z|\psi|^2\int|\psi|^2 dz \to 0$ for $t\to\infty$. Therefore, $E_{\rm tot}(t) \geqslant -NV_R$ for $t\to\infty$. If $g<0$ is sufficiently small, the initial energy is smaller than $-NV_R$. This contradicts the conservation of $E_{\rm tot}$. Therefore, there exists a regime for attractive interactions where assumption (5) does not hold. This scenario is called self-trapping; i.e., at least part of the wave packet is localized in the disorder [13–15]. Note that in this continuous model the spectrum of $\mathcal{L}$ does not have an upper bound. Therefore, the above proof by contradiction does not apply for repulsive interactions. This explains the absence of self-trapping for repulsive interactions.

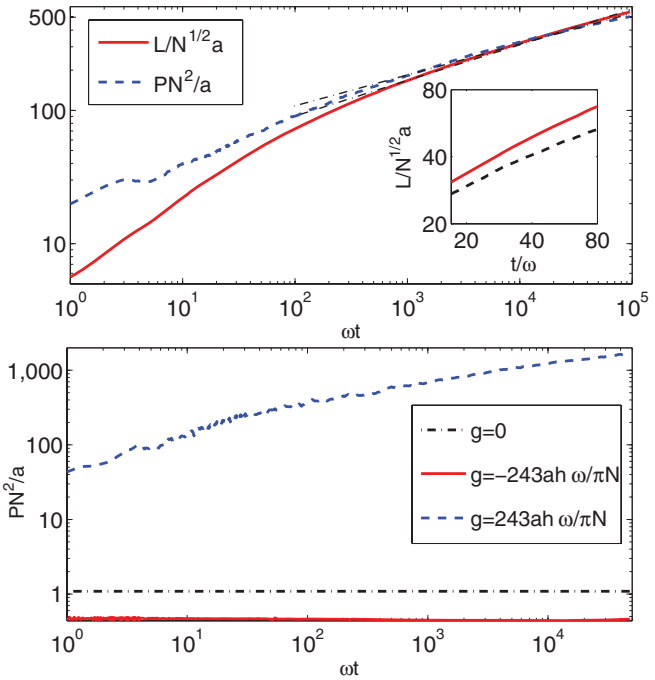

FIG. 3. (Color online) Top panel: Evolution of the rms width L and participation length P [39]. At long times, L and P follow the power laws Eq. (4) with exponents α_1 and α_2 about $0.2 \sim 0.3$ (fit for $10^2/\omega \leqslant t \leqslant 10^5/\omega$). Inset of top panel: L integrated over a space domain $[-4000a, 4000a]$ (red solid) and L integrated up to typical resolution limit of experiments [22] (black dashed; see text). All plots are averaged over 7 realizations. Bottom panel: Evolution of P for the noninteracting case (black dash-dotted), attractive interactions (red solid), and repulsive interactions (blue dashed) with the same NM as initial state. All other parameters are as in Fig. 2.

IV. A HEURISTIC EXPLANATION OF SUBDIFFUSION

We explain the observed values of the subdiffusion exponent with a heuristic model of interaction-induced transitions between NMs. In a noninteracting disordered system, NMs are mutually orthogonal. The interaction breaks this orthogonality and transfers one NM pair to another. Because the transfer rate depends on the density, the transfer rate decreases while the wave packet expands. Based on this picture, various authors have developed heuristic models for subdiffusive expansion by relating the transfer rate to the variation of L and P in different models [14]. We follow Ref. [26], where the authors derived a heuristic model by using the perturbation theory in Ref. [40].

Let us start from the description of the eigenstates, i.e., the NMs, of the operator $\mathcal{L} = -\frac{\hbar^2}{2m}\partial_z^2 + V(z)$. The eigenenergies of NMs lie in $[-V_R,\infty)$. Observing that the stationary

distribution of the momentum has a cutoff $1/\xi_{\rm in}$ [see Eq. (2)], we only consider the NMs with momenta below $1/\xi_{\rm in}$. We order these NMs $\{\phi_\nu\}$ in space along their center-of-mass position $Z_\nu = \int z|\phi_\nu(z)|^2 dz$. We assume that $n(z,t) = |\psi(z,t)|^2$ is constant in an interval with width $l(t)$ at time t. This assumption is reasonable at least for small g since a chapeau appears in the center of the wave packet when g is small (see Sec. III). Because the total particle number is conserved, $n(t)l(t) = N$ and $1/P(t) = \int |\psi|^4 dz = n^2(t)l(t)$. Therefore, $n(t) \propto P^{-1}(t)$ and $l(t) \propto P(t)$. On average there are about $n(t)d$ atoms around a NM. Here, d is the average distance between NMs with momenta below $1/\xi_{\rm in}$. More specifically, d can be defined as $\lim_{I\to\infty} \frac{I}{\mathcal{N}_I}$, where $\mathcal{N}_I$ is the total number of NMs with momenta below $1/\xi_{\rm in}$ in an interval with width I.

The dominant process induced by the two-body interaction is to transfer a NM pair ϕ_{ν_1} and ϕ_{ν_2} to another NM pair ϕ_{ν_3} and ϕ_{ν_4} [40]. The interaction coupling term of this process is

$$V'_{\nu_1\nu_2\nu_3\nu_4} = \frac{gn(t)d}{2} \int \phi^*_{\nu_4}\phi^*_{\nu_3}\phi_{\nu_2}\phi_{\nu_1} dz. \tag{6}$$

From perturbation theory we know that this process can happen only if the energy is conserved; i.e., $\Delta E_{\nu_1\nu_2\nu_3\nu_4} = |\epsilon_{\nu_4} + \epsilon_{\nu_3} - \epsilon_{\nu_2} - \epsilon_{\nu_1}| = 0$. In a disordered system, energy cannot be conserved perfectly. According to the theory in Ref. [40], when

$$R_{\nu_1\nu_2\nu_3\nu_4} = \frac{\Delta E_{\nu_1\nu_2\nu_3\nu_4}}{V'_{\nu_1\nu_2\nu_3\nu_4}} < 1, \tag{7}$$

the transition can still take place. Condition (7) can be considered as the energy conservation condition in a disordered system. The transfer rate associated with this microscopic process is

$$\Gamma_{\nu_1\nu_2\nu_3\nu_4} = \frac{2\pi}{\hbar} \frac{|V'_{\nu_1\nu_2\nu_3\nu_4}|^2}{\Delta E}. \tag{8}$$

The transfer rate Γ of the macroscopic process can be seen as the average of $\Gamma_{\nu_1\nu_2\nu_3\nu_4}$. Denote the probability of quartets $\{\phi_{\nu_1},\phi_{\nu_2},\phi_{\nu_3},\phi_{\nu_4}\}$ that satisfy condition (7) as $p(R_{\nu_1\nu_2\nu_3\nu_4} < 1)$. Then,

$$\Gamma \propto |n(t)p(R_{\nu_1\nu_2\nu_3\nu_4} < 1)|^2. \tag{9}$$

We then relate Γ to the diffusion rate; i.e., $dP^2/dt \propto \Gamma$ [14]. If the probability p of quartets of NMs that satisfy the energy conservation is known, it is possible to obtain the evolution of P from the relation $n(t) \propto 1/P(t)$. As in Ref. [14], we have computed $R_{\nu,\rho_0} = \min_{\rho\neq\nu} R_{\nu\nu\rho}$ for different ν averaged over 50 realizations. We have identified two regimes. In the first regime, analogous to the *strong chaos* regime in Ref. [14], the probability $p(R_{\nu,\rho_0} < 1)$ is independent of $n(t)$. In the second regime, analogous to the *weak chaos* regime in Ref. [14], there exists a scaling law between n and the probability $p(R_{\nu,\rho_0} < 1)$; i.e., $p(R_{\nu,\rho_0} < 1) \propto n$ (see Fig. 4). Therefore, we find $dP^2/dt \propto P^{-2}$ in the *strong chaos* regime and $dP^2/dt \propto P^{-4}$ in the *weak chaos* regime. This leads to $\alpha_2 = 1/4$ (strong chaos) and $\alpha_2 = 1/6$ (weak chaos). This is qualitatively consistent with our numerical results (about $0.2 \sim 0.3$). The inset of the bottom panel of Fig. 4 shows that the pair of NMs ν and ρ_0 which satisfy $R_{\nu,\rho_0} < 1$ have a multipeak structure. This is the same as the situation in the DNLSE [14]. The probability density of the distance between the pair which satisfies $R_{\nu,\rho_0} < 0.1$ for $gn/\hbar\omega = 14$ is shown in the bottom main panel of Fig. 4. We note that correlations in the disorder potential may accelerate the spreading as highlighted in Ref. [26]. Recently, however, this acceleration has been revealed as an effect of intermediate time scales so we do not incorporate correlations into our heuristic model [41].

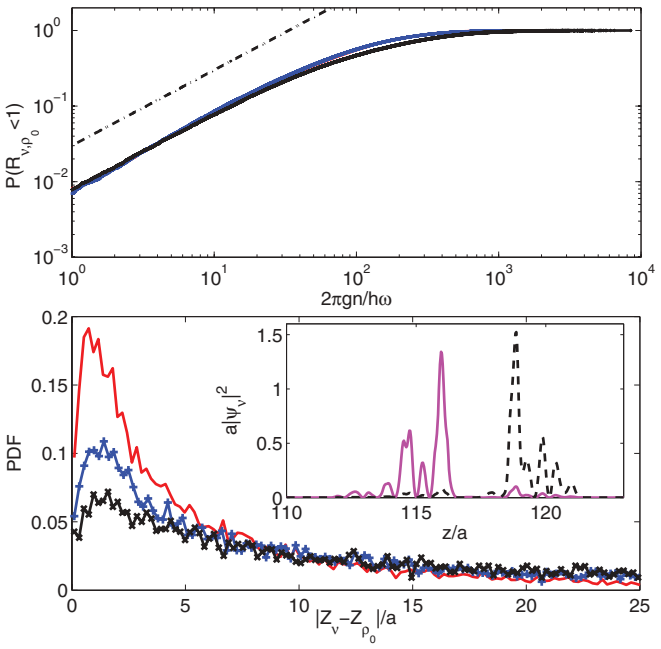

FIG. 4. (Color online) Top panel: Dependence of $p(R_{\nu,\rho_0} < 1)$ on the interaction energy gn averaged over 50 realizations in a domain with width $123a$ (solid lines). The dashed line indicates decay proportional to n. Parameters are $V_R = 0.24\mu$ (black with $\times$), 0.34μ (blue with $+$), 0.48μ [red (indistinguishable)], $\hbar\omega = 0.024\mu, \sigma_R = 0.65\xi_{\rm in}$. Bottom panel: Probability densities (PDF) of the distance between strongest coupling pairs which satisfies $R_{\nu,\rho_0} < 0.1$ for $gn/\hbar\omega = 14$ (colors indicate the same parameters as in the top panel). Inset: Multipeak structure of a typical strongest coupling NM pair (black dashed and magenta lines).

V. EXPERIMENTAL RELEVANCE

Finite camera resolution in *in situ* measurements limits the extent over which the experimenter can obtain the BEC density accurately. This limitation affects the calculation of L and P from measured densities. In order to check the relevance of this effect we have computed $L(t)$ (P) by integrating numerically $z^2|\psi(z)|^2$ $(1/|\psi(z)|^4)$ over (i) a very large z domain ($z \in [-4000a, 4000a]$) and (ii) a domain where $a|\psi(z)|^2/N > 2.72 \times 10^{-4}$ [42]. The result for L at short times is shown in the inset of the top panel of Fig. 3. We observe that the resolution-limited L [case (ii)] differs noticeably from the true value of L [case (i)] even on relatively short time scales (on the order of a few seconds for typical parameters [22]). Our simulations also suggest that the slope of the resolution-limited rms width decreases more prominently over time than the true rms width, which would result in an apparent reduction of diffusion. This is explained by considering the wings of the BEC $|\psi(z,t)|^2 \propto \exp\{-2|z|/L_{\rm loc}\}$ [43]. The maximum of

$z^2|\psi(z,t)|^2$ (kernel of the integration in L) is at $|z| = L_{\rm loc}$. Therefore, L strongly depends on the BEC density near $|z| = L_{\rm loc}$. A typical localization length is $L_{\rm loc} \simeq 0.5$ mm (see experimental results in Ref. [22]). However, this localization length is close to the extent over which the BEC density can be measured at a typical camera resolution (see Fig. 2 in Ref. [22]). Consequently, the long wings of the BEC cannot be measured at this resolution but would contribute markedly to the calculation of the rms width. This effect contributes to the explanation of the apparent discrepancy between our results and the experimental observation of Anderson localization over a few seconds in a speckle potential [22].

Notice that this finite-resolution effect on L originates from the fact that there exist NMs with large localization length [44]. Therefore, if the NMs with large localization length can be suppressed, L can be measured accurately. A way to suppress these NMs is to reduce the interaction coupling constant g, which can be realized via a Feshbach resonance.

We suggest that it is a better choice to measure both L and P in long-time ultracold atom experiments. This is because only measuring the rms width L cannot distinguish full delocalization from partial delocalization (i.e., self-trapping) [13,14]. However, the participation length would provide additional information on whether self-trapping has occurred. Moreover, even if L suffers from finite-size effects when g is large, it is still possible to get some valuable information about the long-time behavior via P because P is more robust than L under the effect of finite camera resolution [45].

VI. GENERALIZED INTERACTIONS AND AN IMPURITY MODEL OF DISORDER

In this section, we generalize the model Eq. (1) by replacing (i) the cubic nonlinearity by $|\psi|^{2\sigma}\psi$ and (ii) the speckle potential by an impurity disorder. Let us start from the dimensionless form of the GPE. We introduce the dimensionless quantities by rescaling lengths with $z \to za$, times with $t \to t/\omega$, energies with $\hbar\omega$, and the wave function with $\psi \to \psi\sqrt{N/a}$, where ω is the longitudinal trapping frequency, $a = \sqrt{\hbar/m\omega}$, and N is the total number of particles. After replacing the cubic nonlinearity and rescaling Eq. (1) without the harmonic trap we have

$$i\partial_t\psi = \left[-\tfrac{1}{2}\partial_z^2 + V_h v(z/\sigma_h) + \beta|\psi|^{2\sigma}\right]\psi, \qquad (10)$$

where $V_h = V_R/\hbar\omega$, $\sigma_h = \sigma_R/a$, and $\beta = gN/a\hbar\omega$. In Fig. 5 we demonstrate subdiffusive spreading for $\sigma = 0.5$. This provides evidence that subdiffusion is not limited to the cubic nonlinearity of the GPE. In fact, subdiffusive spreading should exist for all σ but with a different subdiffusion exponent. This is because different σ lead to different numbers of NMs to be coupled [14]. We note that a similar conclusion for different σ has been obtained in some discrete models [35,46].

For case (ii) we consider the disorder potential

$$V_1(z) = V_0 \sum_j g(z - Z_j), \qquad (11)$$

where $g(z) = \exp(-z^2/2\omega_0^2)$ and $\{Z_j\}$ are random variables. The average distance of a pair taken from $\{Z_j\}$ is denoted by d_0. This impurity model can be implemented by using

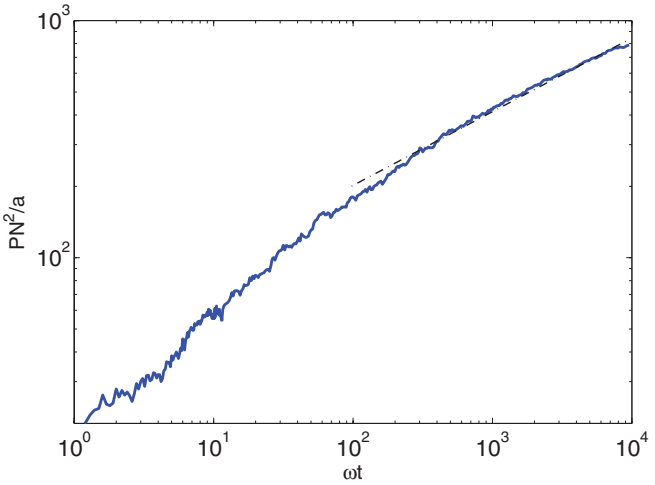

FIG. 5. (Color online) Evolution of the participation length P with generalized contact interaction for $\sigma = 0.5$ for one realization. At long time, P follows a power law with exponent roughly about $0.2 \sim 0.3$ (fit for $10^2/\omega \leqslant t \leqslant 10^4/\omega$). Other parameters are $V_h = 4.86$, $\sigma_h = 0.05$, $\beta = 100$.

impurity atoms in ultracold atomic gases [47,48]. In the limit $\omega_0 \to 0$ and $V_0\omega_0$ fixed, this potential approximates uncorrelated disorder made of a random series of δ peaks used in a number of theoretical investigation of disordered systems [49]. The potential $V_1(z)$ has the mean value

$$\langle V_1\rangle = \sqrt{2\pi}V_0\omega_0/d_0 \qquad (12)$$

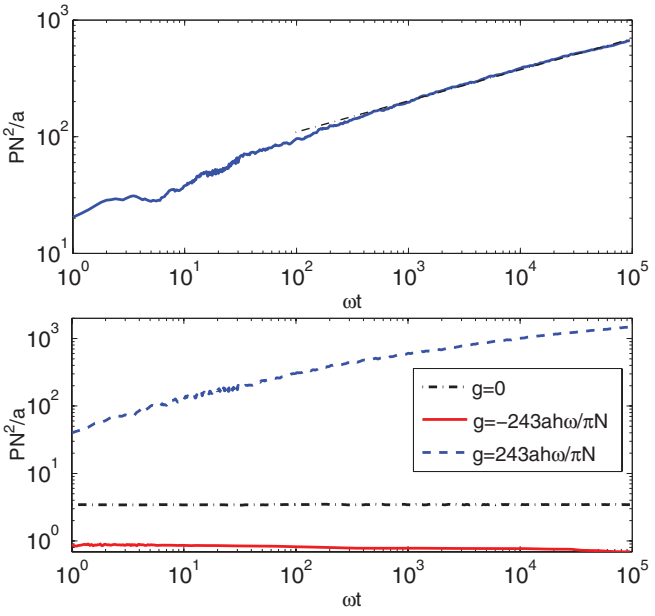

FIG. 6. (Color online) Top panel: Evolution of the participation length P for impurity disorder for one realization. At long times, P follows a power law with exponent α_2 about $0.2 \sim 0.3$ (fit for $10^2/\omega \leqslant t \leqslant 10^5/\omega$). Other parameters are $V_R = 0.12\mu, \hbar\omega = 0.024\mu, \sigma_R = 0.65\xi_{\rm in}, d_0 = a$. Bottom panel: Evolution of P for the noninteracting case (black dashed-dotted), attractive interactions (red solid), and repulsive interactions (blue dashed) with the same initial state (some NM). Other parameters are as the top panel.

and correlation function

$$C(z) = \frac{V_0^2}{d_0} \int g(x)g(x+z)dx = V_R^2 c(z/\sigma_R), \qquad (13)$$

where $V_R = \sqrt{\omega_0/d_0}V_0$, $c(x) = \sqrt{\pi}\exp\{-x^2\}$, and $\sigma_R = 2\omega_0$. The eigenvalue spectrum of the operator $\mathcal{L}_1 = -\frac{\hbar^2}{2m}\partial_z^2 + V_1(z)$ is bounded from below but does not have an upper bound [40]. The localization length of eigenstates with energy ϵ within the Born approximation is given by

$$\xi(\epsilon) = \frac{4\hbar^2}{\pi m}\frac{\epsilon}{V_R^2\sigma_R}e^{k^2\sigma_R^2}, \qquad (14)$$

where $k = \sqrt{2m\epsilon}/\hbar$ [27]. In the top panel of Fig. 6, we show that the impurity disorder potential leads to subdiffusion for long times. The participation length follows a power law at long times with a subdiffusion exponent roughly about $0.2 \sim 0.3$. We also find that self-trapping only exists for attractive interactions as illustrated in the bottom panel of Fig. 6. We note that subdiffusive spreading is also preserved for long times when the external parameters are changed.

VII. SUMMARY AND DISCUSSION

In conclusion, we have studied the long-time dynamics of a continuous 1D BEC in a speckle or impurity disorder potential. We have demonstrated numerically that subdiffusive spreading prevails for relatively long times when AL of the BEC is destroyed. Our model shows self-trapping only for attractive interactions. Furthermore, we have found that generalizing the contact interaction to $|\psi|^{2\sigma}\psi$ also leads to subdiffusive spreading. When the coupling constant is small, this subdiffusive spreading can be interpreted as interaction-assisted hopping between localized NMs by a heuristic model. We have provided a possible explanation of why the rms width saturates in the experiment [22]. We conclude that it is advantageous to measure the participation length in addition to the rms width for studying the long-time behavior of ultracold atoms in disorder potentials.

In contrast to spatially discrete models, in our continuous model we have found that AL in the tails is destroyed on the simulated time scale for typical coupling constants. This is due to the existence of NMs with large localization length in the tails. For future work, it will be interesting to address whether NMs with larger and larger localization length can be excited permanently in the tails. Also, destruction of AL in the tails renders possible the breakdown of existing subdiffusion theories [14,26]. Owing to recent advances in BECs with strong dipolar interactions (for a review, see [50]), another future avenue for our work will be the effect of long-range dipolar interaction on AL [51].

ACKNOWLEDGMENTS

B.M. and T.L. are supported by the NSFC under Grants No. 91130005 and No. 11171009. M.R. and W.B. are supported by the Academic Research Fund of the Ministry of Education of Singapore, Grant No. R-146-000-120-112.

[1] P. W. Anderson, Phys. Rev. **109**, 1492 (1958).
[2] L. Fleishman and P. W. Anderson, Phys. Rev. B **21**, 2366 (1980).
[3] S. A. Gredeskul and Y. S. Kivshar, Phys. Rep. **216**, 1 (1992).
[4] A. Aspect and M. Inguscio, Phys. Today. **62**(8), 30 (2009).
[5] D. M. Basko, I. L. Aleiner, and B. L. Altshuler, Ann. Phys. **321**, 1126 (2006).
[6] Y. Dubi, Y. Meir, and Y. Avishai, Nature (London) **449**, 876 (2007).
[7] Y. Lahini, A. Avidan, F. Pozzi, M. Sorel, R. Morandotti, D. N. Christodoulides, and Yaron Silberberg, Phys. Rev. Lett. **100**, 013906 (2008).
[8] Y. Lahini, R. Pugatch, F. Pozzi, M. Sorel, R. Morandotti, N. Davidson, and Y. Silberberg, Phys. Rev. Lett. **103**, 013901 (2009).
[9] L. Sanchez-Palencia and M. Lewenstein, Nat. Phys. **6**, 87 (2010).
[10] G. Modugno, Rep. Prog. Phys. **73**, 102401 (2010).
[11] D. L. Shepelyansky, Phys. Rev. Lett. **70**, 1787 (1993).
[12] A. S. Pikovsky and D. L. Shepelyansky, Phys. Rev. Lett. **100**, 094101 (2008).
[13] G. Kopidakis, S. Komineas, S. Flach, and S. Aubry, Phys. Rev. Lett. **100**, 084103 (2008).
[14] S. Flach, D. O. Krimer, and Ch. Skokos, Phys. Rev. Lett. **102**, 024101 (2009).
[15] M. Larcher, F. Dalfovo, and M. Modugno, Phys. Rev. A **80**, 053606 (2009).
[16] T. V. Laptyeva, J. D. Bodyfelt, D. O. Krimer, Ch. Skokos, and S. Flach, Europhys. Lett. **91**, 30001 (2010).
[17] J. D. Bodyfelt, T. V. Laptyeva, Ch. Skokos, D. O. Krimer, and S. Flach, Phys. Rev. E **84**, 016205 (2011).
[18] S. Fishman, Y. Krivolapov, and A. Soffer, arXiv:1108.2956.
[19] M. V. Ivanchenko, T. V. Laptyeva, and S. Flach, Phys. Rev. Lett. **107**, 240602 (2011).
[20] L. Sanchez-Palencia, D. Clément, P. Lugan, P. Bouyer, G. V. Shlyapnikov, and A. Aspect, Phys. Rev. Lett. **98**, 210401 (2007).
[21] A. Iomin, Phys. Rev. E **81**, 017601 (2010).
[22] J. Billy, V. Josse, Z. Zuo, A. Bernard, B. Hambrecht, P. Lugan, D. Clément, L. Sanchez-Palencia, P. Bouyer, and A. Aspect, Nature (London) **453**, 891 (2008).
[23] G. Roati, C. D'Errico, L. Fallani, M. Fattori, C. Fort, M. Zaccanti, G. Modugno, M. Modugno, and M. Inguscio, Nature (London) **453**, 895 (2008).
[24] F. Jendrzejewski, A. Bernard, K. Müller, P. Cheinet, V. Josse, M. Piraud, L. Pezzé, L. Sanchez-Palencia, A. Aspect, and P. Bouyer, Nat. Phys. **8**, 398 (2012).
[25] B. Deissler, M. Zaccanti, G. Roati, C. D'Errico, M. Fattori, M. Modugno, G. Modugno, and M. Inguscio, Nat. Phys. **6**, 354 (2010).
[26] E. Lucioni, B. Deissler, L. Tanzi, G. Roati, M. Zaccanti, M. Modugno, M. Larcher, F. Dalfovo, M. Inguscio, and G. Modugno, Phys. Rev. Lett. **106**, 230403 (2011).
[27] L. Sanchez-Palencia, D. Clément, P. Lugan, P. Bouyer, and A. Aspect, New J. Phys. **10**, 045019 (2008).
[28] M. Piraud, P. Lugan, P. Bouyer, A. Aspect, and L. Sanchez-Palencia, Phys. Rev. A **83**, 031603 (2011).

[29] L. Pitaevskii and S. Stringari, *Bose-Einstein Condensation* (Oxford University Press, Oxford, 2003).
[30] W. Bao, D. Jaksch, and P. A. Markowich, J. Comput. Phys. **187**, 318 (2003).
[31] W. Bao and J. Shen, SIAM J. Sci. Comput. **26**, 2010 (2005).
[32] P. J. Channell and C. Scovel, Nonlinearity **3**, 231 (1990).
[33] S. Palpacelli and S. Succi, Phys. Rev. E **77**, 066708 (2008).
[34] P. Lugan, A. Aspect, L. Sanchez-Palencia, D. Delande, B. Grémaud, C. A. Müller, and C. Miniatura, Phys. Rev. A **80**, 023605 (2009).
[35] C. Skokos and S. Flach, Phys. Rev. E **82**, 016208 (2010).
[36] F. Wegner, Z. Phys. B **36**, 209 (1980).
[37] We note that perhaps 7 realizations are not enough to get an accurate estimate of the subdiffusion exponent for long times. However, as in Ref. [12], a rough estimate up to one digit precision is probably trustworthy. We also note that the time scale (up to $10^5/\omega$) may not be large enough to show the true asymptotic behavior. However, a qualitative conclusion (i.e., power-law behaviors of rms width and participation length) for long times should be reliable.
[38] I. García-Mata and D. L. Shepelyansky, Phys. Rev. E **79**, 026205 (2009).
[39] The reason why $L/N^{1/2}a$ and PN^2/a are presented in Fig. 3 is that we compute the dimensionless wave function $\sqrt{a/N}\psi(z)$ in numerics.
[40] I. L. Aleiner, B. L. Altshuler, and G. V. Shlyapnikov, Nat. Phys. **6**, 900 (2010).
[41] M. Larcher, T. V. Laptyeva, J. D. Bodyfelt, F. Dalfovo, M. Modugno, and S. Flach, arXiv:1206.0833.
[42] This value is obtained from the experiment Ref. [22] where $a = 4.64\ \mu$m, $N = 1.7 \times 10^4$, and the resolution is 1 atom/μm.
[43] In fact, the far wings deviate from this form (see Ref. [28]). Nevertheless, this formula is a very good candidate to fit experimental data in Ref. [22].
[44] In discrete models [13–15,26], this effect does not exist because the localization length of NMs is only several lattice spacings.
[45] In the top panel of Fig. 3, we find that P is distinguishable from resolution-limited participation length. This is because P is determined by the bulk part (near $|z| = 0$) of the density profile, which has a very narrow width.
[46] T. V. Laptyeva, J. D. Bodyfelt, and S. Flach, Europhys. Lett. **98**, 60002 (2012).
[47] U. Gavish and Y. Castin, Phys. Rev. Lett. **95**, 020401 (2005).
[48] B. Paredes, F. Verstraete, and J. I. Cirac, Phys. Rev. Lett. **95**, 140501 (2005).
[49] I. M. Lifshitz, S. A. Gredeskul, and L. A. Pastur, *Introduction to the Theory of Disordered Systems* (Wiley, New York, 1988).
[50] T. Lahaye, C. Menotti, L. Santos, M. Lewenstein, and T. Pfau, Rep. Prog. Phys. **72**, 126401 (2009).
[51] C. Albrecht and S. Wimberger, Phys. Rev. B **85**, 045107 (2012).